THE JOURNAL OF PHYSICAL CHEMISTRY C

Article

pubs.acs.org/JPCC

Tuning the Redox Coupling between Quantum Dots and Dopamine in Hybrid Nanoscale Assemblies

Xin Ji,[†] Nikolay S. Makarov,[‡] Wentao Wang,[†] Goutam Palui,[†] Istvan Robel,[‡] and Hedi Mattoussi*[,†]

[†]Department of Chemistry and Biochemistry, Florida State University, 95 Chieftan Way, Tallahassee, Florida 32306, United States

[‡]Center for Advanced Solar Photophysics, Chemistry Division, Los Alamos National Laboratory, Los Alamos, New Mexico 87545, United States

Supporting Information

ABSTRACT: We explored the charge transfer interactions between CdSe−ZnS core−shell quantum dots (QDs) and the redox active neurotransmitter dopamine, using covalently assembled QD−dopamine conjugates. We combined steady-state fluorescence, time-resolved fluorescence, and transient absorption bleach measurements to probe the effects of changing the QD size (thus the QD energy levels) and the conjugate valence on the rate of QD photoluminescence quenching when the pH of the medium was adjusted from acidic to alkaline. We measured substantially larger quenching efficiencies, combined with more pronounced shortening of the carrier dynamics of these assemblies for smaller size QDs and in alkaline pH. Moreover, we found that changes in the QD size alter the electron and hole relaxation of photoexcited QDs but with different extents. For instance, a pronounced change in the hole relaxation was measured in alkaline buffers. Moreover, the hole relaxation was faster for conjugates of green-emitting QDs as compared to their red-emitting counterparts. We attribute these results to the more favorable electron transfer rates from the reduced form of the dopamine to the valence band of the QDs, a process that becomes more efficient for green-emitting QDs. The latter benefits from lower oxidation potential and larger energy mismatch with the green QDs in alkaline buffers. In comparison, the effects of pH changes on the rates of electron transfer from excited QDs to dopamine are less affected by the QD size. These findings reflect the importance of the energy mismatch between the QD energy levels and the redox levels of dopamine, and shed light onto the complex interactions involved in these assemblies. Such conjugates also provide promising sensing and imaging tools for use in *in vivo* experiments.

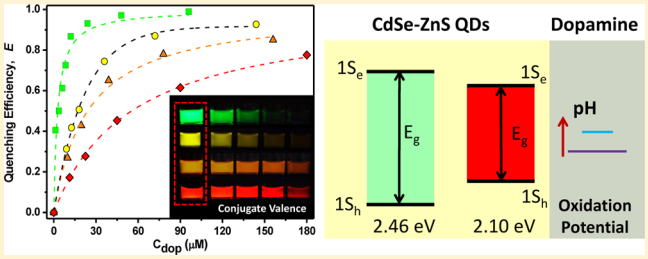

INTRODUCTION

One of the key photophysical characteristics of semiconductor quantum dots is the size- and composition-dependence of their absorption and emission properties.[1−8] CdSe−ZnS core−shell quantum dots, for example, exhibit broad absorption spectra with large extinction coefficients, and narrow emission profiles that can be tuned over a wide optical range, with high photoluminescence (PL) quantum yield and a remarkable photo and chemical stability.[9−11] They are also in a size regime where the effects of surface-bound molecules can seriously influence their overall physical and chemical behaviors. The photophysical properties of these materials can further be altered by closely coupled dyes and fluorescent proteins, due to resonance energy transfer interactions, which alter the electron−hole recombination rates in the nanocrystals.[12−18] Luminescent QDs were also shown to interact strongly with proximal metal- and redox-active complexes, via charge transfer (CT) interactions, which can result in pronounced changes in the QD photoemission and absorption properties.[19−22] Guyot-Sionnest and co-workers were the first to explore the ability of reducing molecules (sodium biphenyl) to induce a pronounced bleaching of the first absorption peak of CdSe QDs due to electron injection from the redox molecules into the conduction band of the nanocrystals.[23,24] They further correlated that with losses in the QD PL signal and measured intraband transitions promoted by excitation of these injected electrons with weak energy photons (wavelength of 3−6 μm).[23] Since then, several groups have also shown that QDs can engage in pronounced charge transfer interactions with redox active molecules in a variety of configurations, including interactions with redox active biological complexes.[20,25−29]

In addition to probing changes in the steady-state and time-resolved PL, charge transfer interactions can also be effectively investigated using time-resolved transient absorption (TA) spectroscopy. These measurements probe the effects of redox level alignments and separation-distance between the QD and the proximal complexes on the charge transfer interactions.[30−36] In one example, Kamat and co-workers elucidated the size-dependent electron injection rates from several sets of photoexcited CdSe QDs (with diameter ranging from 7.5 to 2.4 nm) to TiO_2 nanocrystals, in close-packed thin films.[31] They reported an enhancement in the electron transfer rate with

Received: November 7, 2014
Revised: January 7, 2015
Published: January 14, 2015

DOI: 10.1021/jp511178u
J. Phys. Chem. C 2015, 119, 3388−3399

decreasing QD diameter. In particular, they proposed that by varying the QD size, it is possible to modulate the rate of electron transfer between CdSe and TiO_2, which can be exploited for light harvesting in solar cells.[31] In another example, Lian and co-workers probed the interactions between CdS QDs and Rhodamine B using transient absorption measurements.[37] They found that, in addition to interactions driven by energy transfer, charge transfer from the QD to the proximal Rhodamine B can simultaneously occur via electron transfer to the unoccupied orbital and/or hole transfer to the occupied orbital of the complex. Such process was facilitated by the relative alignment of the redox potential of Rhodamine B with respect to the energy levels of the QD. They also showed that the electron transfer rate could be controlled by changing the QD size and/or the number of molecules attached to the QD surface.

In a previous study, we investigated the charge transfer interactions between CdSe−ZnS QDs and dopamine, a redox active complex with pH and oxygen-dependent properties.[27,28] In particular, we have shown that for a set of yellow-emitting QDs the PL losses depend on the number of dopamine groups arrayed around the QD surface, as well as the medium pH.[28] We have also used time-resolved transient absorption spectroscopy to characterize the charge transfer interactions in such a system, and found that they involve charge transfer between the QDs and two forms of the catechol that coexist at equilibrium in the medium: (1) electron transfer from photoexcited QDs to the oxidized quinone; and (2) electron transfer from the reduced form of the dopamine (catechol) to the valence band of photoexcited QDs.[28] We should stress that redox interactions with dopamine represent a challenging fundamental problem to understand, due to their dependence on pH and oxygen. Dopamine exhibits exceedingly complex redox properties with the medium pH, involving 2-proton and 2-electron transformation of the 2-hydroxyl group, and it is predicted to have two pK_a values occurring at pH of 9.3 and 12.6.[38] Dopamine and its derivatives are also highly relevant in chemical biology because these neurotransmitters play critical functions involving brain activity and behavior, including cognition, motivation, sleep, attention, and learning.[39−41]

To gain a better insight into the mechanisms that drive the PL quenching of the QDs, we expanded the above studies using different sets of QDs with distinct band gaps. For this, we prepared four different sets of CdSe−ZnS QDs with emission peaks at λ_{max} = 525 nm (green), 573 nm (yellow), 590 nm (orange), and 610 nm (red). These nanocrystals were transferred to buffer media via cap exchange using bidentate ligands made of dihydrolipoic acid appended with a short PEG chain, followed by covalent coupling via amine-to-isothiocyanate reaction using dopamine-isothiocyanate (dopamine-ITC) as shown in Figure 1.[42] In these QD−dopamine complexes, the center-to-center separation distance was fixed, by using ligands with a given PEG length (Figure 1). We measured a pronounced PL quenching combined with shortening of the PL lifetime. These changes were found to strongly depend on three distinct parameters: (1) the conjugate valence, (2) the pH of the buffer used, with substantially larger quenching measured in alkaline media than in acidic dispersions, and (3) the QD size, with much weaker PL losses measured for red-emitting QDs than for their green-emitting counterparts.

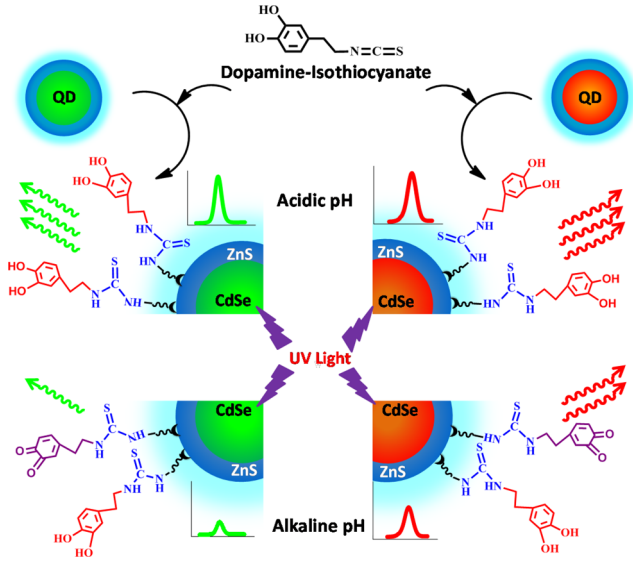

Figure 1. Schematic representation of two sets of QD−dopamine conjugates prepared using green-emitting QDs (left) and red-emitting QDs (right). The schematics show the effects of changing the pH from acidic to alkaline, which materializes in a decrease in the oxidation potential of the dopamine along with a partial chemical transformation of a few catechols to quinones in the QD-conjugates. The anticipated changes in the QD PL emission are shown in the insets. Higher quenching is measured for green-emitting QDs and in alkaline buffers.

RESULTS AND DISCUSSION

Effects of Valence and QD Size. *a. Steady-State Fluorescence.* Figure 2 shows representative PL spectra collected from green- (a), yellow- (b), orange- (c), and red-emitting (d) QDs for several dopamine-ITC-to-QD molar ratios. Here, the QD dispersions refer to nanocrystals ligand-exchanged with a mixture of 95:5 DHLA-PEG_{750}-OCH_3:DHLA-PEG_{600}-NH_2, while control samples refer to dispersions of QDs prepared with 100% DHLA-PEG_{750}-OCH_3. For these dopamine-ITC-to-amine molar ratios, we used the molar concentration of amine groups in the dispersion extracted from the QD concentration and the anticipated number of ligands per nanocrystal (see below).[28,44] We should note that when preparing the QD-conjugates, the concentrations of dopamine-ITC added to each set of QD dispersions were slightly higher for larger size QDs, so that the overall dopamine-ITC-to-amine molar ratio in the medium stays the same for the four sets of QDs studied. This is done to account for the small differences in the overall number of ligands per QD (number of surface ligands is $\propto R^2$ for spherical QDs), and guarantees that the first-order bimolecular reaction analysis applies to our assemblies.[45] The dopamine-ITC concentration added to each sample was based on estimates of the number of DHLA-PEG ligands per QD, as done in our previous report.[28,44] Although the exact count of the number of ligands seems to depend on the conditions and system used, the structure of the ligands, and the analytical techniques used (e.g., NMR or optical spectroscopy), most studies have shown that the number of ligands linearly tracks the overall surface area per nanocrystal. For our QD−ligand system, previous studies have shown that the density of these bidentate PEGylated ligands tracks changes on the nanocrystal surface (as expected), with footprint area (FPA) per ligand of ~1.25 nm^2.[44] This implies the density of DHLA-PEG ligands is ~100−200 ligands per

DOI: 10.1021/jp511178u
J. Phys. Chem. C 2015, 119, 3388−3399

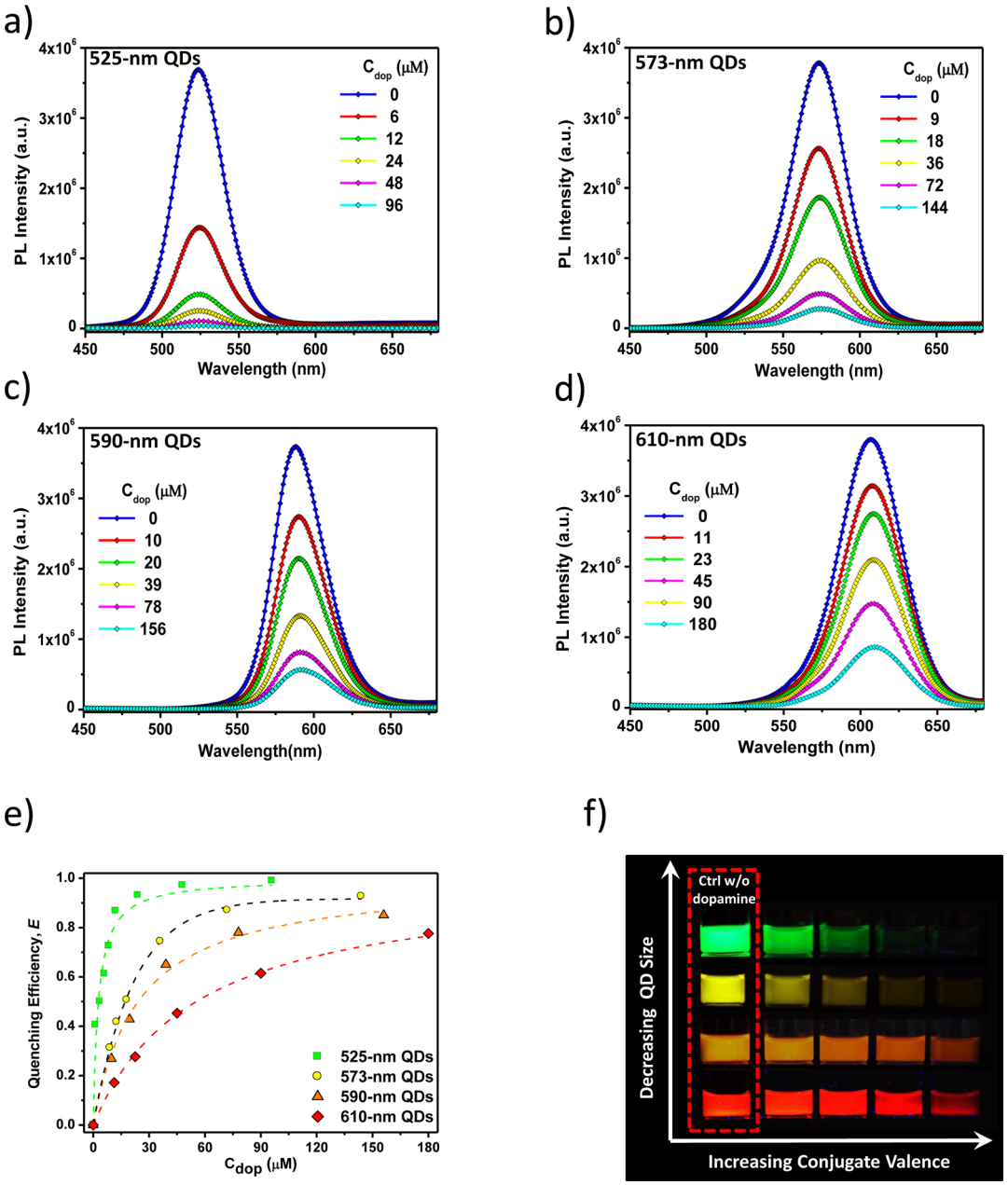

Figure 2. PL spectra collected from QD−dopamine conjugates dispersed in DI water (pH is ~6.5) for increasing concentration of dopamine-ITC: (a) 525 nm green-, (b) 573 nm yellow-, (c) 590 nm orange-, and (d) 610 nm red-emitting QDs. (e) Quenching efficiency versus C_{dop} for different size QDs along with fits using eq 1; the experimental values were extracted from the PL data using eq 7a. The QD concentration in these dispersions was ~32 nM. An additional fit of the quenching efficacy versus valence accounting for the Poisson correction is provided in the Supporting Information (Figure S5) for the green QDs. (f) A fluorescence image of selected dispersions of these QD-conjugates under UV illumination. The QD concentration in these dispersions was ~0.8 μM.

QD for the above nanocrystals. Ligand counting is still a challenge for these systems,[46] and recent developments in analytical tools based on spectroscopic techniques such as NMR, thermogravimetric analysis (TGA), and optical absorption should provide valuable information about such a parameter in the future.[47−49]

The data show a progressive loss in the QD PL with increasing concentration of dopamine-ITC for the four sets of QDs used. However, the PL losses were largest for the green-emitting QDs and decreased for the yellow, orange, and were smallest for the red-emitting QDs (see Figure 2e). The fluorescence images of selected dispersions of these conjugates under UV illumination, shown in Figure 2f, provide a visual confirmation of the size-dependent PL quenching measured for the sets of QDs used. The data shown in Figure 2e indicate that, although the exact values of the quenching efficiency depend on the set of QDs used, the overall trend is consistent with a centro-symmetric QD-dopamine conjugate configuration (see Figure 1); each conjugate is made of a central QD surrounded by several dopamine groups arrayed at a fixed average separation distance, r, from the QD center. Indeed, the trend for E versus C_{dop} can be easily fit to an expression of the form:[28]

DOI: 10.1021/jp511178u
J. Phys. Chem. C 2015, 119, 3388−3399

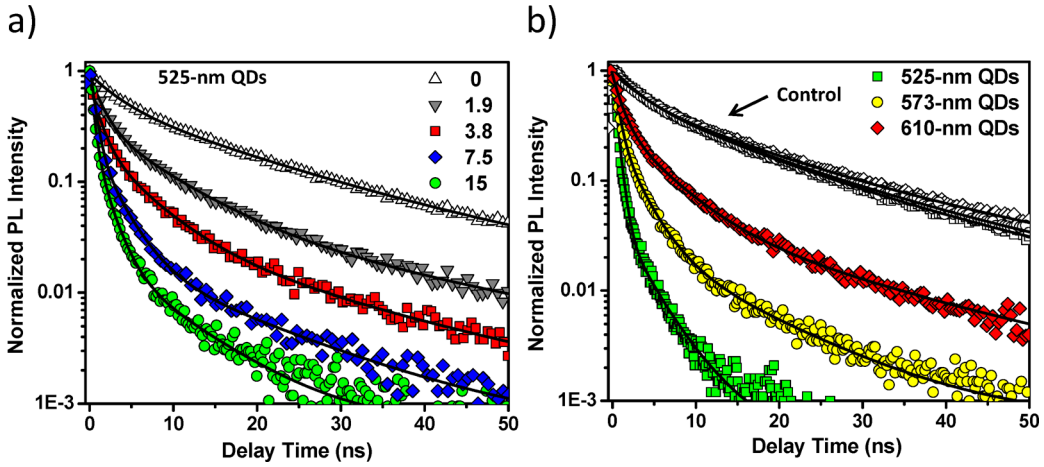

Figure 3. (a) Normalized time-resolved PL decays collected from QD−dopamine conjugates (525 nm-emitting QDs) for various dopamine-ITC-to-amine molar ratios (indicated in the legend). (b) Normalized time-resolved PL decays of three QD−dopamine conjugates made using different size QDs and a fixed dopamine-ITC-to-amine molar ratio of 30:1; green-, yellow-, and red-emitting are shown. The profiles for the control dispersions of the three sets of QDs are shown (empty symbols). Lines are fit to the data using eq 5.

$$E = \frac{\alpha' C_{dop}}{\alpha' C_{dop} + K} \tag{1}$$

where α' and K are experimental parameters that respectively depend on the relative alignment of the redox levels of the dopamine with respect to the energy bands of the QD, as well as the separation distance. Here, we should note that the K value could additionally be affected by the changes in the QD size, even when the same PEG bridge is used for all samples. For instance, red-emitting dots would produce slightly larger separation distance, because they have slightly bigger core size; the effects of QD size on the overall quenching are small, nonetheless. Such behavior is fully consistent with the predicted expression for the dependence of E versus conjugate valence, n, given by[20,28]

$$E = \frac{\alpha n}{\alpha n + K} \tag{2}$$

Here, α is directly related (proportional) to α'.[28] Because heterogeneity in the conjugate valence is rather an inherent property of nanopartricle-conjugates, the dependence of the quenching efficiency on the dopamine-to-QD ratio (valence, n) could be best fitted by accounting for the heterogeneity using the Poisson statistics and an equation of the form:[50]

$$E(N) = \sum_{n=1}^{N} p(n, N)E(n) \quad \text{with} \quad p(n, N) = N^n \frac{e^{-N}}{n!} \tag{3}$$

where N is the average dopamine-to-QD ratio used and n is the exact number of dopamine groups attached to a single QD. The Poisson distribution function, $p(n,N)$, accounts for heterogeneity in the conjugate valence, and $E(n)$ is given by eq 2 above.[50] Below we show that while eq 3 provides a better fit for the experimental data for the green-emitting QDs, more simplified eqs 1 and 2 can be used to fit the data collected from dispersions of the larger (red-emitting) QDs.

Equation 2 is similar to what is predicted and measured for FRET (Förster resonance energy transfer)-induced quenching in these centro-symmetric donor−acceptor assemblies, such as QD−protein−dye conjugates.[43] The conversion of eq 1 (for E vs C_{dop}) to eq 2 (for E vs n) is correct, because the number of coupled dopamines per QD in the final assemblies (after purification) is proportional to the concentration of dopamine-ITC used in the reaction, due to the fact that amine-to-ITC coupling obeys the first-order bimolecular reaction.[45,51] The data shown in Figure 2e indicate that the PL quenching substantially varies from one set of QDs to another. For instance, the PL of green QDs is nearly fully quenched at C_{dop} = 30 μM with E exceeding 0.9. Conversely, at C_{dop} = 30 μM, the quenching efficiency measured for the other samples is 0.6 for the yellow, 0.5 for the orange QDs, and only 0.3 for the red QDs. Saturation in the measured E values for the larger size QDs is reached at much higher concentrations of added dopamine. Fitting the data in Figure 2e to eq 1 yields values for K/α' = 2.8, 14.3, 23.1, and 55.3 for the green-, yellow-, orange-, and red-emitting QDs, respectively.[28] This indicates that the highest quenching efficiency is measured for the set of QDs with the largest band gap (smallest size). The quenching efficiency then progressively decreases for QDs with smaller band gap (or increasing size). We should note that fitting the quenching data using the Poisson correction (eq 3 instead of eq 2) improves the agreement with the experimental data for the green-emitting QDs, where the PL losses are higher due to more efficient interactions. A side-by-side fit to the data for green-emitting QDs using eqs 2 and 3 (fit accounting for the Poisson distribution) is provided in the Supporting Information, Figure S5. No sensible improvement could be observed when fitting the other data shown in Figure 2e. This agrees with what has been demonstrated for FRET interactions with QDs, where the importance of accounting for the Poisson distribution is mostly relevant for donor−acceptor pairs with high spectral overlap and short separation distances.[50]

b. Time-Resolved Fluorescence. Figure 3a shows a representative plot of the normalized time-resolved PL decays collected for a series of green-emitting QDs with varying conjugate valence. Clearly, a pronounced shortening of the PL lifetime (as compared to control dispersion), commensurate with the increase in the conjugate valence, is observed; additional data for the red-emitting QDs are provided in the Supporting Information (Figure S2). Conversely, Figure 3b shows the normalized time-resolved fluorescence decay profiles of three different-size QDs at the same valence (corresponding to a nominal dopamine-ITC-to-amine molar ratio of 30:1).

DOI: 10.1021/jp511178u
J. Phys. Chem. C 2015, 119, 3388−3399

Data show that shortening of the PL lifetime varies with the set of QDs used, with a substantially faster decay measured for the smaller nanocrystals and vice versa; that is, shortening of the PL lifetime as compared to the control sample is the largest for the green-emitting QDs, smaller for the yellow-, and smallest for the red-emitting QDs. Furthermore, the quenching efficiency values extracted from the time-resolved data using eq 7b are comparable to those shown in Figure 2e. For instance, for dispersions made of green QD-conjugates, the average exciton lifetime decreased from τ_D = 19.87 for unconjugated QDs to τ_{DA} = 1.42 ns for conjugates prepared using a dopamine-ITC-to-amine ratio = 30:1; the corresponding quenching efficiency is E = 0.93. Conversely, this lifetime decreased from τ_D = 20.43 ns to τ_{DA} = 8.99 ns (corresponding to E = 0.56) for the red-emitting QDs. Negligible changes in the exciton lifetimes were measured for control samples made of 100% methoxy-PEG-QDs mixed with dopamine and purified as above, indicating that no coupling between QDs and dopamine-ITC has taken place in those samples.[28] Clearly, the time-resolved fluorescence measurements complement the steady-state data summarized in Figure 2.

The above data on the PL lifetime decays can be used to extract estimates for the charge transfer rate constant (k_{CT}) defined as[31,52,53]

$$k_{CT} = \frac{1}{\tau_{DA}} - \frac{1}{\tau_D} \quad (4)$$

The corresponding experimental values, summarized in Table 1, show that for QD−dopamine conjugates with comparable

Table 1. Experimental Values for the Charge Transfer Rate Constant (k_{CT}) for All Four Sets of QDs Extracted from the Time-Resolved Fluorescence Measurements and Fits to Equation 4[a]

	control dispersion	dopamine-ITC:amine = 30:1		dopamine-ITC:amine = 7.5:1	
QDs $\lambda_{abs/max}$ (nm)	τ_D (ns)	τ_{DA} (ns)	k_{CT} (s^{-1})	τ_{DA} (ns)	k_{CT} (s^{-1})
505	19.87	1.42	6.54×10^8	8.17	7.21×10^7
552	20.34	4.51	1.73×10^8	10.24	4.85×10^7
567	21.12	6.40	1.09×10^8	12.40	3.33×10^7
590	20.43	8.99	6.23×10^7	14.95	1.79×10^7

[a]The conjugates were prepared with a nominal dopamine-ITC:amine ratio of 30:1 and 7.5:1 in DI water.

valence (i.e., prepared with a dopamine-ITC-to-amine molar ratio of 30:1 or 7.5:1), the charge transfer rate constant decreases with increasing QD size. For instance, there is a 10-fold increase in the charge transfer rate constant from red- to green-emitting QDs for the conjugates prepared with a dopamine:QD ratio of 30:1 (i.e., from 6.23×10^7 s^{-1} for the 610 nm QDs to 6.54×10^8 s^{-1} for the 525 nm QDs), a result consistent with the sizable difference in the quenching efficiency data shown in Figure 2.

Effects of Solution pH. The effects of buffer pH on the interactions between QD and proximal dopamine were probed by tracking the changes in three physical processes: (1) steady-state fluorescence, (2) time-resolved fluorescence, and (3) visible transient absorption (or visible TA bleach) probed with femtosecond excitation. The time-resolved fluorescence was used to probe two complementary processes and required two independent measurements. One measurement probed the PL decay with ∼100 ps resolution and was carried out using the TCSPC experimental setup. The other measurement was used to probe the excitation decay with picosecond resolution associated with the band edge relaxation of the hole; the measurement was carried out using a streak camera. Conversely, the TA bleach measurement was used to probe the electron relaxation dynamics.[30,54] All of these effects were investigated when the pH of the medium was adjusted from pH 4 (acidic) to pH 10 (alkaline). In these measurements, we maintained the same conjugate valence for all samples, by fixing the dopamine-ITC-to-amine molar ratio at ∼7.5:1. This ratio was selected because it results in a PL quenching far from the saturation regime for all sets of QDs (see Figure 2).[28] For the TA bleach and streak camera measurements, we focused on two QD samples emitting at 525 nm (green, largest band gap) and at 610 nm (red, smallest band gap) as the observed differences are more pronounced for the "extreme" QD sizes. We should note that at pH 4, the reduced form of the complex (catechol) is dominant, while at pH 10 the molar fraction of the oxidized form (i.e., quinone) is substantially higher.

a. Steady-State Fluorescence Measurements. Figure 4a shows the cumulative plot for the relative progression of the integrated PL intensity with changes in solution pH for all four sets of QD-conjugate dispersions. The corresponding PL spectra are provided in the Supporting Information (Figure S3). The pH effects can be summarized as follow: (1) The QD PL undergoes a progressive decrease when the pH is changed from acidic to alkaline, with substantially larger quenching efficiency measured in alkaline media than in acidic dispersions for all samples. (2) Larger PL quenching efficiencies are measured for solutions made with smaller QDs, and vice versa. (3) Control dispersions made of 100% DHLA-PEG-methoxy-QDs exhibit no changes in the PL throughout the pH range. A visual rendition of the PL changes is provided in the fluorescence image shown in the inset of Figure 4a, where several dispersions of green- and red-emitting QD-dopamine conjugates at pH ranging from 4 to 10 are illuminated at 365 nm using a hand-held UV lamp. These results complement and expand our previous measurements reported in ref 28.

b. Nanosecond Time-Resolved Fluorescence Measurements. To complement the steady-state data, we probed the pH-induced changes in the PL lifetimes using the TCSPC setup. Data collected for assemblies with green-emitting QDs are shown in Figure 4; additional data on the time-resolved fluorescence signal for dispersions of red-emitting QD-conjugates are provided in the Supporting Information (Figure S4). We found that when the pH was adjusted from pH 4 to pH 10 a sizable change in the time-resolved PL decay was measured for QD-assemblies (Figure 4b). Furthermore, the effects of such pH increase on the PL decay were much more pronounced for assemblies with green-emitting QDs (as shown in Figure 4b and Supporting Information Figure S4). In comparison, little to no change in the decay was observed for unconjugated QDs (control) when the solution pH was adjusted.

The above experimental time-resolved fluorescence data can also be used to extract information on the dependence of the charge transfer rate constant (k_{CT}) on the pH of the buffer used. Table 2 shows that the changes in k_{CT} values with pH are much larger for green-emitting QDs than for their red-emitting counterparts. This further confirms the steady-state PL data and

DOI: 10.1021/jp511178u
J. Phys. Chem. C 2015, 119, 3388−3399

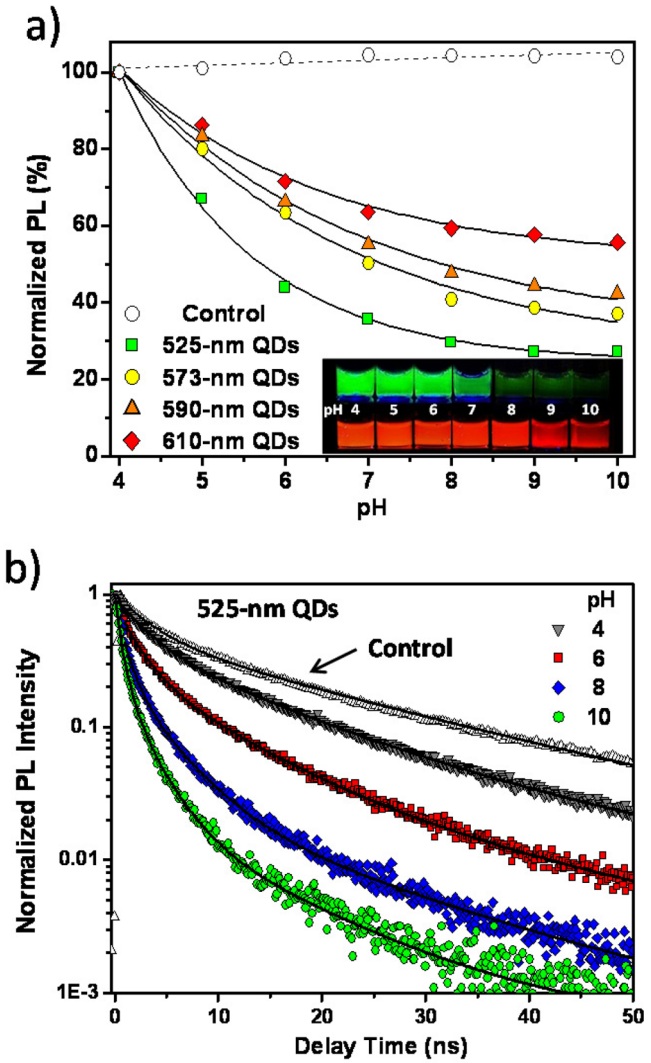

Figure 4. (a) PL intensity for the pH range 4−10, normalized with respect to initial values at pH 4, measured for all sets of QD-conjugates prepared with a nominal dopamine-ITC-to-amine ratio of 7.5. Control experiments were carried out by using 100% DHLA-PEG-methoxy at a range of pH from 4 to 10 (dash line); only one control (one QD size) is shown here; the PL changes with pH measured for the control were very small (<8%). Inset shows the fluorescence images of selected dispersions of green- and red-emitting QD-conjugates dispersed in different pH buffers; samples were illuminated at 365 nm using a hand-held UV lamp. (b) Normalized time-resolved PL decay curves for green-emitting QD−dopamine complexes and QDs alone dispersed in pH 4, 6, 8, and 10 buffers collected using TCSPC.

Table 2. Experimental Values for the Charge Transfer Rate Constant (k_{CT}) for Green- and Red-Emitting QDs Derived from the Time-Resolved Fluorescence Measurements[a]

	green QDs; $\lambda_{abs/max}$ = 505 nm		red QDs; $\lambda_{abs/max}$ = 590 nm	
samples	τ_{DA} (ns)	k_{CT} (s^{-1})	τ_{DA} (ns)	k_{CT} (s^{-1})
control	20.85 (τ_D)		18.12 (τ_D)	
pH 4	17.59	8.89×10^6	16.65	4.87×10^6
pH 6	11.74	3.72×10^7	15.88	7.78×10^6
pH 8	7.20	9.09×10^7	14.89	1.20×10^7
pH 10	4.83	1.59×10^8	14.69	1.29×10^7

[a]The conjugate samples were prepared with a nominal dopamine-to-amine ratio of 7.5:1. Control corresponds to data collected at pH 4.

complements results from previous studies on the dependence of the dopamine redox activity on pH.[28]

c. Visible Time-Resolved Transient Absorption. We have performed visible transient absorption measurements to probe whether or not the observed charge transfer interactions are dominated by electron transfer from the QDs to quinone. As the 1S exciton TA bleach is dominated by the state filling of the 1S electron level, with negligible contribution from the hole, probing the kinetics of the transient absorption at the first absorption peak will thus provide information on the 1S electron depopulation kinetics.[34] Such measurements allow us to test the effects of the conjugation on the conduction band electrons.[52,55] For this, the bleach decays were measured at 500 nm for the green-emitting QDs and at 600 nm for the red-emitting QDs. Furthermore, because electron transfer is anticipated to take place between photoexcited QDs and the oxidized form of the complex (namely quinone),[28] these effects will be much better accounted for by performing the TA bleach measurements using QD-conjugates in alkaline solutions (at pH 10), where the concentration of quinone groups is expected to be larger.[38] Figure 5 shows a side-by-side comparison of the TA decay for green- (a) and red-emitting (b) QD−dopamine conjugates together with data for unconjugated QDs dispersed in pH 10 buffers. The data show that there is a slightly faster decay in the TA bleach signals upon conjugation to dopamine. However, the amount of changes measured between the two sets of QDs is rather small. This implies that the electron transfer is only slightly affected by the size of QDs at this time scale in alkaline media. The corresponding lifetimes are 410 and 43 ps for green-emitting QDs and their corresponding QD-conjugates, respectively. In contrast, the lifetimes are 245 ps for red QDs (control) and 77 ps for the conjugates at pH 10. These lifetimes can be used to extract estimates for the charge transfer rates, k_{et}, for the two sets of QDs using a relationship similar to eq 4 ($k_{et} = \tau_{DA}^{-1} - \tau_D^{-1}$), with $k_{et} = 2.08 \times 10^{10}$ s^{-1} for green QD-conjugates and $k_{et} = 8.90 \times 10^9$ s^{-1} for the red QD-conjugates. This indicates a slightly faster decay rate (~2 times) for green-emitting QDs as compared to their red counterparts. This change is smaller than what was measured for the overall charge transfer rate (k_{CT}) at pH 10 shown in Table 2. Thus, the changes in the PL dynamics measured in the same scale (see below) can be attributed to changes in the hole relaxation. Nonetheless, at the longer time scale (1−20 ns), the charge transfer rate is more affected by the size of the QDs used when the pH of the medium is changed, as indicated by the time-resolved fluorescence data shown in Figure 4 and Table 2.

d. Picosecond Time-Resolved Fluorescence Measurements. To probe the effects of the pH on the hole relaxation, we performed time-resolved photoluminescence measurements in the same time window as the above-mentioned transient absorption experiments. Because the effects of QD size on the electron decay in this time scale are very small (see above section and Figure 5), we can relate the measured changes in the time-resolved PL decay to changes in the hole relaxation of photoexcited QDs due to the interactions with the catechol groups (reduced form of the complex). This argument can also be discussed within the context of hole transfer from the QD to the occupied orbital of the complex. Figure 6 shows side-by-side plots of the normalized PL decay for the green- and red-emitting QDs, unconjugated (control) and QD−dopamine assemblies, at pH 4 and pH 10. At pH 10 the difference in time-resolved PL decays is more pronounced for the green-emitting QDs, consistent with the data above. At pH 4 a sizable

DOI: 10.1021/jp511178u
J. Phys. Chem. C 2015, 119, 3388−3399

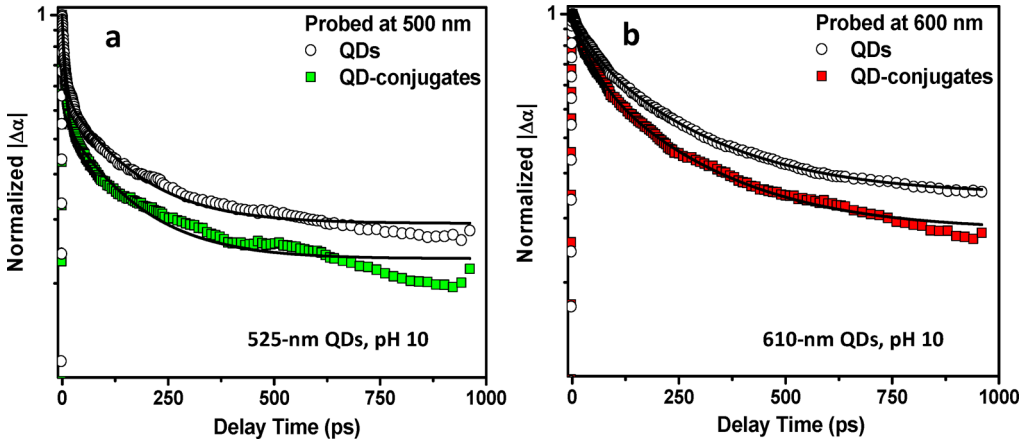

Figure 5. Decay of the visible transient absorption (TA) signal at the first exciton peak of the following: (a) Green-emitting QDs probed at 500 nm; the corresponding lifetimes are 410 ps for QDs and 43 ps for QD-conjugates. (b) Red-emitting QDs probed at 600 nm; the corresponding lifetimes are 245 ps for QDs control and 77 ps for the conjugates. Data were collected at pH 10. All conjugates samples were prepared at a nominal dopamine-to-amine ratio of 7.5.

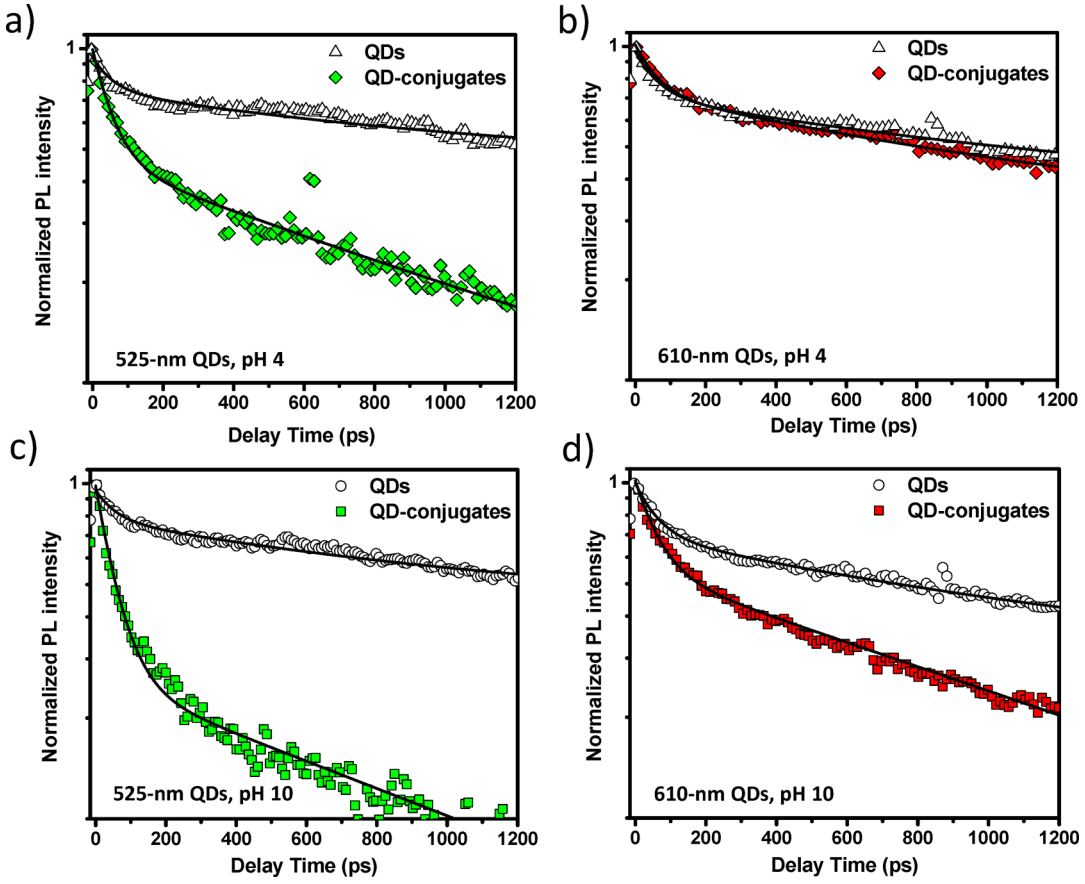

Figure 6. Normalized time-resolved PL decay profiles (transient PL) for green- and red-emitting QD-dopamine complexes and QDs alone dispersed in buffer with pH 4 (a,b) and pH 10 (c,d), collected using a streak camera. All conjugates samples were prepared at a nominal dopamine-to-amine ratio of 7.5.

shortening of the relaxation times is measured for the green-emitting QDs, but only a marginal change is measured for the red-emitting QDs as compared to control dispersions (see Figure 6a,b). This suggests that the hole transfer from the QDs to dopamine is less efficient for the large-size QDs in acidic conditions. These results clearly indicate that changes in the buffer pH mostly alter the hole relaxation in the QD–dopamine conjugates, with substantially larger changes measured for nanocrystals with a wider energy band gap. We should note that the two time-resolved techniques have an inherent fundamental difference. While transient absorption probes the whole population of the QDs in the sample, transient PL mainly probes the highly emissive QDs at long time scale and all of the species at short time scale. This should not affect the information extracted about the nature of the charge transfer interactions and their response to changes in the

DOI: 10.1021/jp511178u
J. Phys. Chem. C 2015, 119, 3388−3399

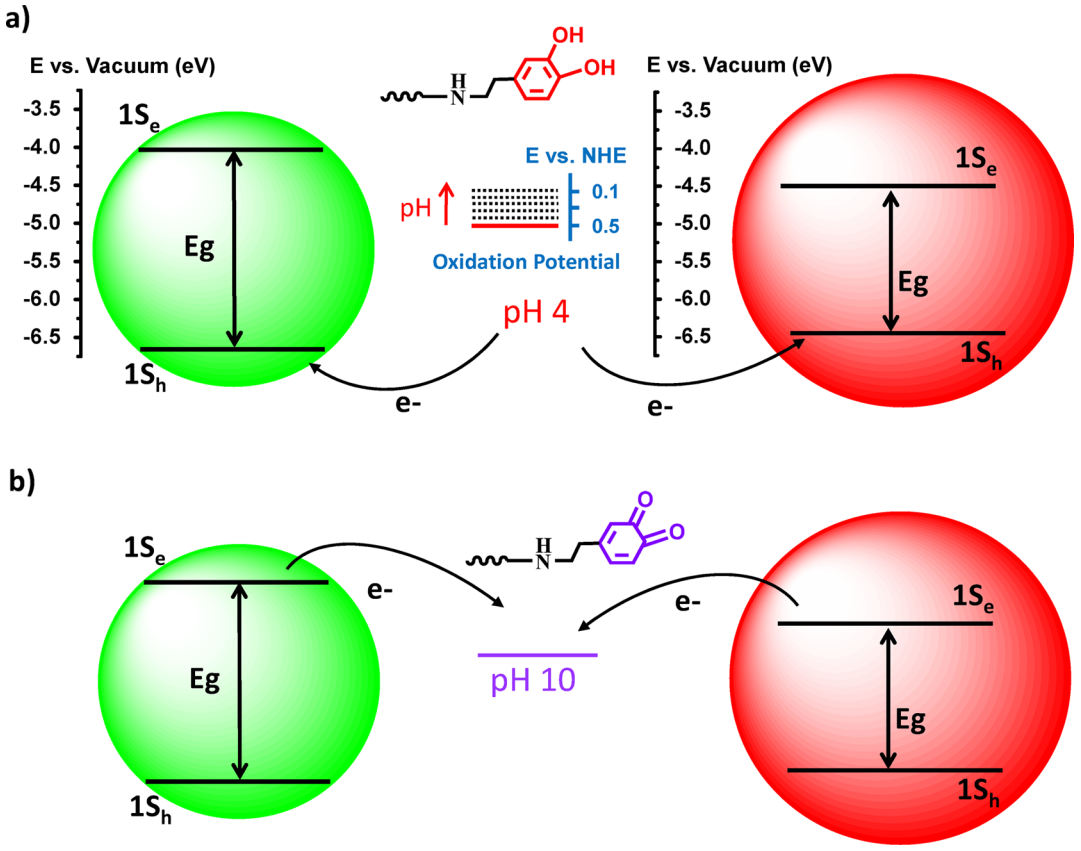

Figure 7. Schematic representation of the proposed charge transfer mechanism (involving electron and hole carriers) in acidic and alkaline media for the two sets of QD-conjugates: wider band gap green QDs and narrower band gap red QDs. Rationales depicted in (a) and (b) are based on a combination of picosecond TR fluorescence data collected using a streak camera and TA bleach data collected for both QD sizes at pH 4 and pH 10. The redox levels of dopamine were obtained by using cyclic voltammograms for dispersions of dopamine-PEG-methoxy in buffer media.[28] The corresponding energy levels of two sets of CdSe–ZnS QDs with respect to the electrochemical scale were extracted from ref 1. These were based on a Fermi level for CdSe of −5.78 eV, a bandgap of 1.75 eV, giving a conduction band at ∼ −4.905 eV and a valence band at ∼ −6.655 eV. The energy levels of the cetechols were extracted from the *C*–*V* data (reported in ref 28) and using the relation $E_{ox} = -4.5\ \text{eV} - eE_f$, where E_f is the oxidation potential measured with respect to NHE.[66] We should note that the energy levels for CdSe reported in ref 3 are slightly different from the ones we used here and originally described in ref 1.

QD size or buffer pH. As clearly shown, the contributions from hole and electron relaxations can be separated in these experiments and the contribution from electrons is much less pronounced.

Proposed Mechanism for the Charge Transfer Interactions and Induced PL Quenching. The main findings from our measurements can be summarized as follows: Chemically coupling dopamine to a fluorescent CdSe–ZnS QD drastically alters the photoemission properties of the nanocrystal, as verified by steady-state and time-resolved fluorescence measurements. The PL quenching tracks the valence of the QD–dopamine conjugates, but more importantly the quenching efficiency can be strongly influenced by the energy levels of the nanocrystals, with substantially higher efficiencies measured for wider bandgap dots, and vice versa. The rate of fluorescence quenching also depends on the pH of the buffer used, with more pronounced PL losses measured in alkaline solutions. The use of time-resolved fluorescence and TA measurements, to separately probe the relaxation of the carriers, provides additional insights into how changing the buffer pH can alter the electron and hole relaxation in these complexes. We find that faster relaxations of the hole carrier are measured in alkaline solutions. Moreover, shortening of these relaxations is more pronounced for conjugates made with wider energy band gap (e.g., using green-emitting QDs). Conversely, the effects of QD size on the electron relaxation are smaller. We have also previously identified that the PL quenching in these assemblies could not be attributed to Förster resonance energy transfer between the nanocrystals and dopamine, because there is no measurable spectral overlap between the QD emission and dopamine absorption; the absorption of dopamine is weak, limited to the UV region of the spectrum, and does not overlap with the PL profile of any of the QDs used.[28] These results cannot be attributed to simple physisorption or complexation of the dopamine onto the metal surface of the QDs. Indeed control experiments showed that when 100% methoxy-QDs or nonreactive dopamine (no ITC) were used, only very small PL quenching was measured due to solution phase (collision) interactions.[28] Furthermore, after one round of purification using a filtration device, to remove the small dopamine molecules from the dispersions, the measured residual quenching was negligible (consistently smaller than 5%). This result indicates that complexing or physisorption of the redox complex on the QDs is negligible, presumably due to the strong coordination of the DHLA-PEG ligands on the QDs and shielding of the nanocrystal surfaces.[28]

We attribute the above findings to interactions between the nanocrystals and bound dopamine that are dominated by

DOI: 10.1021/jp511178u
J. Phys. Chem. C 2015, 119, 3388–3399

charge transfer processes, as schematically detailed in Figure 7a,b. More precisely, we propose that a photoexcited QD does not interact with a homogeneous redox complex in the medium. Instead, it experiences interactions with two distinct species that coexist within the same conjugate:[28] (1) The first involves electron transfer from the reduced form of dopamine (catechol, a natural electron donor) to the valence band of photoexcited QDs (this can also be viewed as hole transfer from the QD to the catechol). This electron-donating capacity of the catechol is inferred from previous cyclic voltammetry data collected from dopamine solutions, where a well-defined oxidation peak was measured. Furthermore, that peak progressively shifts to lower values when the pH is switched from acidic to basic.[28] This electron transfer from the catechol to a photoexcited QD alters the relaxation of the holes in a pH-dependent manner (as a significantly higher relative concentration of catechol is present at acidic pH). The decrease in the oxidation potential of dopamine at alkaline pH's is also accompanied by a shift of the thermodynamic equilibrium toward higher concentrations of the oxidized catechol, that is, a propensity of dopamine to more easily oxidize combined with an increase in the relative concentration of quinone in the medium. (2) The second interaction involves electron transfer between photoexcited QDs and quinone. The latter naturally results from oxidation of the catechol in a process catalyzed by oxygen; its concentration is higher in alkaline solutions (but extremely small in acidic solutions). This alters the relaxation of the 1S electron, and produces faster decay at higher pH.[28] We should note that the QD energy levels shown in Figure 7a are slightly different from those depicted in ref 28. We think that the levels shown here and extracted from ref 1 represent a more accurate description of the system.

The effects of varying the QD size (or energy bandgap) on the electron and hole transfer rates and their dependence on the solution pH are complex. At pH 4 interactions of the QD with the catechol may dominate due to low concentration of the quinone. Furthermore, at pH 4 changes in the hole relaxation upon conjugation are much larger for the green-emitting QDs (see Figure 6a,b). When the pH is switched to alkaline, the rate of hole decay is increased (i.e., lifetime is shortened) for both sets of QDs, but the change is still more pronounced for green-emitting QDs (see Figure 6c,d). These two features are attributed to larger mismatch between the oxidation level of dopamine and the valence band of the QDs; such mismatch also increases when the pH of the medium becomes more basic. Conversely, the effects of changing the QD size and solution pH on the interaction with the quinone are somewhat less pronounced. Indeed, the TA bleach data show that changes in the relaxation signal from red to green QDs are rather small. This may be attributed to the fact that the shift of the conduction band of the QDs is not large enough to substantially alter the rate of electron transfer to the redox complex. It can also imply that the reduced form of the complex still dominates the interactions with the valence band for the anticipated number of complexes per QD−dopamine conjugate.

The data collected for the four sets of QDs summarized in Figures 2−6 complement the previous results and interpretation reported previously.[25−28] The charge transfer mechanism controlling the PL changes in these hybrid assemblies as a function of QD size, valence, and pH involves an electron hole "exchange" between QD and dopamine, resulting in QD exciton annihilation, and manifesting in rather large PL quenching efficiencies. Moreover, these CT interactions can be easily and controllably tuned by a combination of changing the QD size and/or composition, because both parameters can affect the energy bandgap. It can also be controlled via conjugate valence and pH of the solution.

CONCLUSION

We combined the use of steady-state and time-resolved fluorescence along with transient absorption bleach measurements to probe the charge transfer interactions between semiconductor QDs and the redox active dopamine, in covalently assembled QD−dopamine conjugates. In particular, we explored the effects of varying the QD size (thus the conduction and valence energy levels), the number of dopamine groups per QD-conjugate (valence), and, more importantly, the effects of adjusting the pH of the medium from acidic to alkaline, on the QD PL quenching.

We recorded higher PL quenching efficiencies and more pronounced shortening in the PL lifetime, when wider bandgap QDs and/or alkaline solutions were used. We attributed these findings to charge transfer interactions between the QDs and two forms of the redox complex that coexist in equilibrium in the medium. (1) The first is interactions between photoexcited QDs and the reduced form of the complex (catechol) via electron transfer from the dopamine to the valence band of the QDs. This pathway becomes more efficient when the medium pH is switched to alkaline conditions, as the oxidation potential of the complex is lowered with increasing pH. It is also stronger for smaller size QDs due to the larger energy mismatch between the redox potential of the complex and the valence band of the QDs. (2) The second is electron transfer interactions between QDs and the oxidized form of the complex (quinone). This pathway also promotes stronger interactions and higher PL quenching in alkaline media. Nonetheless, the measured changes in the rates of electron charge transfer from excited QDs to dopamine are less affected by the QD size when the pH of the medium is made more basic. Conversely, the effects of reducing the QD size on the hole relaxation are substantially more pronounced in alkaline buffers and for green-emitting QDs.

These QD−dopamine assemblies provide an interesting and scientifically challenging problem for exploring the importance of charge transfer interactions in inorganic−biological hybrids. They also shed light onto the complex interactions involved in these assemblies. Our QD−dopamine conjugates coupled via a PEG bridge provide flexible redox-active fluorescent platforms with a great potential for integration in biological systems where effects of pH and redox interactions are crucial. These include potential use for intracellular sensing and vasculature imaging.

EXPERIMENTAL SECTION

Synthesis and Functionalization of Quantum Dots. We prepared four sets of CdSe−ZnS core−shell QDs with the lowest energy absorption (band edge) peak, λ_{abs} = 505, 552, 567, and 590 nm (see Supporting Information, Figure S1). The core−shell QDs were prepared in two reaction steps (CdSe core growth followed by ZnS-overcoating) via reduction of organometallic precursors at high temperature. Growth of the CdSe core involved the reduction of cadmium and selenium precursors at high temperature (300−350 °C) in a coordinating solvent mixture made of trioctyl phosphine (TOP), trioctyl

DOI: 10.1021/jp511178u
J. Phys. Chem. C 2015, 119, 3388−3399

phosphine oxide (TOPO), phosphonic acid, and alkylamines; the CdSe nanocrystal size was controlled via small variations in the precursor concentrations and annealing temperature.[56−59] Overcoating of the CdSe core with ZnS shell was carried out at lower temperature (150−180 °C) using zinc and sulfur precursors.[9−11,59] All QDs were prepared to have a similar thickness ZnS layer; thus, the overall size difference of the core−shell structures is mainly due to changes in the core radius. The nanocrystal sizes were estimated by combining data from three complementary techniques: a correlation between the size extracted from small-angle X-ray scattering and the first absorption peak, along with analysis of transmission electron microcopy (TEM) data.[57,60] The average radii for these nanocrystals are ∼2.8 nm for the green-, ∼3.4 nm for the yellow-, ∼3.6 nm for the orange-, and ∼4.0 nm for the red-emitting QDs.

The hydrophobic QDs (TOP/TOPO-capped) were rendered hydrophilic via ligand exchange using dihydrolipoic acid appended with polyethylene glycol (DHLA-PEG). A small fraction of reactive amine groups was introduced on the QD surface by performing the ligand exchange using a mixture of DHLA-PEG$_{600}$-NH$_2$ (amine-modified reactive ligand) and DHLA-PEG$_{750}$-OCH$_3$ (inert terminated ligand).[61−63] In this particular study, we used a mixture of 95% DHLA-PEG$_{750}$-OCH$_3$ and 5% DHLA-PEG$_{600}$-NH$_2$ (95:5 OCH$_3$:NH$_2$) ligands for all QD samples. Additional details on the ligand synthesis, purification, and characterization can be found in previous references.[62,63]

Assembly of the QD−Dopamine Conjugates. The QD−dopamine assemblies were formed by reacting amine-functionalized QDs (amine-QDs) with dopamine isothiocyanate (dopamine-ITC) for 3.5 h (as schematically shown in Figure 1). Briefly, 100 μL of 5% amine-QDs (initial QD conc. = 8 μM) was added to a vial containing the desired molar amount of dopamine-ITC dissolved in DI water to a total volume of 1 mL and a final QD concentration ∼0.8 μM. Solutions of dopamine-ITC in water were prepared starting with the desired molar amounts of dopamine-ITC predissolved in DMSO. The dopamine-ITC concentration in each sample was adjusted to account for the difference in the number of amine groups per nanocrystal from one set of QDs to another, with slightly higher amounts of dopamine added to dispersions of larger size QDs. For example, the range of dopamine-ITC:QD molar ratios used for preparing dispersions of green-emitting QDs varied between 7.5:1 and 120:1, while molar ratios ranging from 14:1 to 225:1 were used for the red-emitting QD-conjugates. This adjustment maintains a similar reactivity between the dopamine-ITC and amine on the QD for all samples. The mixture was stirred for 3.5 h in the dark at room temperature, followed by removal of excess unreacted dopamine by applying one round of concentration/dilution using a membrane filtration device with Mw Cut-off of 50 kDa (from Millipore). To adjust the solution pH, aliquots (40 μL) of the QD-conjugate (stock) dispersions were mixed with 960 μL of phosphate buffer (10 mM) at the desired pH before the florescence spectra were collected. Additional details about the synthesis of the dopamine-ITC, characterization, along with the coupling strategy can be found in previous references.[28,62,64] The samples stayed homogeneous and aggregation-free after several months of storage at 4 °C. The transient absorption data were collected using dispersions of QDs and QD-conjugates prepared as above but at higher concentrations (∼40−50 μM). The dispersions were first concentrated in DI water and then diluted in the desired pH buffer before data were collected.

Data Collection and Analyses. *Absorption and Fluorescence.* The absorption spectra for all samples were recorded using a UV−vis absorption spectrophotometer (UV 2450 model from Shimadzu). These spectra were used to determine the QD concentration in the samples.[65] The steady-state fluorescence spectra were collected on a Fluorolog-3 spectrometer (HORIBA Jobin Yvon Inc., Edison, NJ), equipped with a fast TBX PMT detector and an air cooled CCD camera. All of the steady-state PL spectra were collected using excitation at 350 nm.

Time-Resolved Fluorescence. Two sets of time-resolved (TR) fluorescence decays profiles were collected using two complementary experimental setups, one spanning 0−100 ns range and the other allowing picosecond resolution and spanning a time range of 0−1500 ps.

The first set of visible TR fluorescence was collected and analyzed using a Time Correlation Single Photon Counting (TCSPC) system integrated in the same Fluorolog-3 above. A pulsed excitation signal with a repetition rate of 1 MHz at 440 nm, provided by a NanoLED-440LH (100 ps, fwhm), was used for sample excitation. The second set of TR PL data was collected using a streak camera (Hamamatsu C5680). The pulsed laser excitation signal at 400 nm was generated by the second harmonic of a fundamental 1 kHz amplified laser system (Spectra-Physics Spitfire). The instrument response function (IRF) was measured to be ∼20 ps fwhm.

The fluorescence decay traces of the QD−dopamine conjugates (and control QDs) in both measurements were fitted with a three-exponential function:

$$I(t) = A_1\, e^{-t/\tau_1} + A_2\, e^{-t/\tau_2} + A_3\, e^{-t/\tau_3} \tag{5}$$

Here, t is time and A_i is a weighting parameter associated with each decay time, τ_i. An average amplitude-weighted lifetime, τ_{avg}, was extracted from the fit as

$$\tau_{avg} = \frac{\sum A_i \tau_i^2}{\sum A_i \tau_i} \tag{6}$$

The PL quenching efficiency, E, was extracted from the steady-state or time-resolved fluorescence data, using the expressions:

$$E = 1 - \frac{F_{DA}}{F_D}, \quad \text{for steady-state fluorescence} \tag{7a}$$

and

$$E = 1 - \frac{\tau_{DA}}{\tau_D}, \quad \text{for time-resolved fluorescence} \tag{7b}$$

where F_{DA} and F_D designate the steady-state (ensemble) PL intensity measured for dispersions of QD−dopamine conjugates and QDs alone (control, without dopamine complexes), respectively. Similarly, τ_{DA} and τ_D, respectively, designate the average exciton lifetime measured for dispersions of the QD-conjugates and for dispersions of QDs alone (control).

Transient Absorption. Transient absorption spectra were recorded using Lab View-controlled home-build setup with the 400 nm ∼100 fs excitation (the same as that used for the measurements with the streak camera above) and white light super continuum probe. Bleach decays were measured for the green- and red-emitting sets of QDs at the first exciton peak (the $1S_e-1S_h$ transition) to monitor electron dynamics. The

DOI: 10.1021/jp511178u
J. Phys. Chem. C 2015, 119, 3388−3399

TA decay traces for the QD-assemblies were fitted using a three-exponential function as done above for the PL data.

■ ASSOCIATED CONTENT

Supporting Information

Additional experimental details. This material is available free of charge via the Internet at http://pubs.acs.org.

■ AUTHOR INFORMATION

Corresponding Author

*E-mail: mattoussi@chem.fsu.edu.

Notes

The authors declare no competing financial interest.

■ ACKNOWLEDGMENTS

X.J., W.W., G.P., and H.M. thank FSU, the National Science Foundation (Grant No. 1058957), and Pfizer for financial support. N.S.M. and I.R. were supported by the Center for Advanced Solar Photophysics, an Energy Frontier Research Center funded by the Office of Basic Energy Sciences, Office of Science, U.S. Department of Energy. We also thank Victor Klimov for the fruitful discussions.

■ REFERENCES

(1) Netherco, Ah. Prediction of Fermi Energies and Photoelectric Thresholds Based on Electronegativity Concepts. *Phys. Rev. Lett.* **1974**, *33*, 1088−1091.

(2) Alivisatos, A. P. Semiconductor Clusters, Nanocrystals, and Quantum Dots. *Science* **1996**, *271*, 933−937.

(3) Nozik, A. J.; Memming, R. Physical Chemistry of Semiconductor−Liquid Interfaces. *J. Phys. Chem.* **1996**, *100*, 13061−13078.

(4) Murray, C. B.; K, C. R.; Bawendi, M. G. Synthesis and Characterization of Monodisperse Nanocrystals and Close-Packed Nanocrystal Assemblies. *Annu. Rev. Mater. Sci.* **2000**, *30*, 545−610.

(5) Talapin, D. V.; Lee, J. S.; Kovalenko, M. V.; Shevchenko, E. V. Prospects of Colloidal Nanocrystals for Electronic and Optoelectronic Applications. *Chem. Rev.* **2010**, *110*, 389−458.

(6) Klimov, V. I. *Nanocrystal Quantum Dots*, 2nd ed.; CRC Press: Boca Raton, FL, 2010; p xv, 469 p.

(7) Smith, A. M.; Nie, S. M. Semiconductor Nanocrystals: Structure, Properties, and Band Gap Engineering. *Acc. Chem. Res.* **2010**, *43*, 190−200.

(8) Amelia, M.; Impellizzeri, S.; Monaco, S.; Yildiz, I.; Silvi, S.; Raymo, F. M.; Credi, A. Structural and Size Effects on the Spectroscopic and Redox Properties of CdSe Nanocrystals in Solution: The Role of Defect States. *ChemPhysChem* **2011**, *12*, 2280−2288.

(9) Hines, M. A.; Guyot-Sionnest, P. Synthesis and Characterization of Strongly Luminescing Zns-Capped CdSe Nanocrystals. *J. Phys. Chem* **1996**, *100*, 468−471.

(10) Dabbousi, B. O.; RodriguezViejo, J.; Mikulec, F. V.; Heine, J. R.; Mattoussi, H.; Ober, R.; Jensen, K. F.; Bawendi, M. G. (CdSe)ZnS Core-Shell Quantum Dots: Synthesis and Characterization of a Size Series of Highly Luminescent Nanocrystallites. *J. Phys. Chem. B* **1997**, *101*, 9463−9475.

(11) Reiss, P.; Bleuse, J.; Pron, A. Highly Luminescent CdSe/ZnSe Core/Shell Nanocrystals of Low Size Dispersion. *Nano Lett.* **2002**, *2*, 781−784.

(12) Snee, P. T.; Somers, R. C.; Nair, G.; Zimmer, J. P.; Bawendi, M. G.; Nocera, D. G. A Ratiometric CdSe/ZnS Nanocrystal pH Sensor. *J. Am. Chem. Soc.* **2006**, *128*, 13320−13321.

(13) Chen, Y.; Thakar, R.; Snee, P. T. Imparting Nanoparticle Function with Size-Controlled Amphiphilic Polymers. *J. Am. Chem. Soc.* **2008**, *130*, 3744−3745.

(14) Yildiz, I.; Deniz, E.; Raymo, F. M. Fluorescence Modulation with Photochromic Switches in Nanostructured Constructs. *Chem. Soc. Rev.* **2009**, *38*, 1859−1867.

(15) Medintz, I. L.; Mattoussi, H. Quantum Dot-Based Resonance Energy Transfer and Its Growing Application in Biology. *Phys. Chem. Chem. Phys.* **2009**, *11*, 17−45.

(16) Sadhu, S.; Haldar, K. K.; Patra, A. Size Dependent Resonance Energy Transfer between Semiconductor Quantum Dots and Dye Using FRET and Kinetic Model. *J. Phys. Chem. C* **2010**, *114*, 3891−3897.

(17) Credi, A. Quantum Dot-Molecule Hybrids: A Paradigm for Light-Responsive Nanodevices. *New J. Chem.* **2012**, *36*, 1925−1930.

(18) Dennis, A. M.; Rhee, W. J.; Sotto, D.; Dublin, S. N.; Bao, G. Quantum Dot−Fluorescent Protein Fret Probes for Sensing Intracellular pH. *ACS Nano* **2012**, *6*, 2917−2924.

(19) Sykora, M.; Petruska, M. A.; Alstrum-Acevedo, J.; Bezel, I.; Meyer, T. J.; Klimov, V. I. Photoinduced Charge Transfer between CdSe Nanocrystal Quantum Dots and Ru-Polypyridine Complexes. *J. Am. Chem. Soc.* **2006**, *128*, 9984−9985.

(20) Medintz, I. L.; Pons, T.; Trammell, S. A.; Grimes, A. F.; English, D. S.; Blanco-Canosa, J. B.; Dawson, P. E.; Mattoussi, H. Interactions between Redox Complexes and Semiconductor Quantum Dots Coupled Via a Peptide Bridge. *J. Am. Chem. Soc.* **2008**, *130*, 16745−56.

(21) Amelia, M.; Font, M.; Credi, A. Luminescence Quenching in Self-Assembled Adducts of $[Ru(Dpp)_3]^{2+}$ Complexes and CdTe Nanocrystals. *Dalton Trans.* **2011**, *40*, 12083−12088.

(22) Stewart, M. H.; Huston, A. L.; Scott, A. M.; Efros, A. L.; Melinger, J. S.; Gemmill, K. B.; Trammell, S. A.; Blanco-Canosa, J. B.; Dawson, P. E.; Medintz, I. L. Complex Forster Energy Transfer Interactions between Semiconductor Quantum Dots and a Redox-Active Osmium Assembly. *ACS Nano* **2012**, *6*, 5330−5347.

(23) Wang, C. J.; Shim, M.; Guyot-Sionnest, P. Electrochromic Nanocrystal Quantum Dots. *Science* **2001**, *291*, 2390−2392.

(24) Shim, M.; Guyot-Sionnest, P. N-Type Colloidal Semiconductor Nanocrystals. *Nature* **2000**, *407*, 981−983.

(25) Clarke, S. J.; Hollmann, C. A.; Zhang, Z. J.; Suffern, D.; Bradforth, S. E.; Dimitrijevic, N. M.; Minarik, W. G.; Nadeau, J. L. Photophysics of Dopamine-Modified Quantumdots and Effects on Biological Systems. *Nat. Mater.* **2006**, *5*, 409−417.

(26) Cooper, D. R.; Suffern, D.; Carlini, L.; Clarke, S. J.; Parbhoo, R.; Bradforth, S. E.; Nadeau, J. L. Photoenhancement of Lifetimes in CdSe/ZnS and CdTe Quantum Dot-Dopamine Conjugates. *Phys. Chem. Chem. Phys.* **2009**, *11*, 4298−4310.

(27) Medintz, I. L.; Stewart, M. H.; Trammell, S. A.; Susumu, K.; Delehanty, J. B.; Mei, B. C.; Melinger, J. S.; Blanco-Canosa, J. B.; Dawson, P. E.; Mattoussi, H. Quantum-Dot/Dopamine Bioconjugates Function as Redox Coupled Assemblies for in Vitro and Intracellular pH Sensing. *Nat. Mater.* **2010**, *9*, 676−684.

(28) Ji, X.; Palui, G.; Avellini, T.; Na, H. B.; Yi, C.; Knappenberger, K. L.; Mattoussi, H. On the pH-Dependent Quenching of Quantum Dot Photoluminescence by Redox Active Dopamine. *J. Am. Chem. Soc.* **2012**, *134*, 6006−6017.

(29) Freeman, R.; Finder, T.; Bahshi, L.; Gill, R.; Willner, I. Functionalized CdSe/ZnS Qds for the Detection of Nitroaromatic or Rdx Explosives. *Adv. Mater.* **2012**, *24*, 6416−6421.

(30) Burda, C.; Link, S.; Mohamed, M.; El-Sayed, M. The Relaxation Pathways of CdSe Nanoparticles Monitored with Femtosecond Time-Resolution from the Visible to the IR: Assignment of the Transient Features by Carrier Quenching. *J. Phys. Chem. B* **2001**, *105*, 12286−12292.

(31) Robel, I.; Kuno, M.; Kamat, P. V. Size-Dependent Electron Injection from Excited CdSe Quantum Dots into TiO_2 Nanoparticles. *J. Am. Chem. Soc.* **2007**, *129*, 4136−4137.

(32) Huang, J.; Stockwell, D.; Huang, Z. Q.; Mohler, D. L.; Lian, T. Q. Photoinduced Ultrafast Electron Transfer from CdSe Quantum Dots to Re-Bipyridyl Complexes. *J. Am. Chem. Soc.* **2008**, *130*, 5632−5633.

(33) Kongkanand, A.; Tvrdy, K.; Takechi, K.; Kuno, M.; Kamat, P. V. Quantum Dot Solar Cells. Tuning Photoresponse through Size and Shape Control of CdSe-TiO_2 Architecture. *J. Am. Chem. Soc.* **2008**, *130*, 4007−4015.

DOI: 10.1021/jp511178u
J. Phys. Chem. C 2015, 119, 3388−3399

(34) McArthur, E. A.; Morris-Cohen, A. J.; Knowles, K. E.; Weiss, E. A. Charge Carrier Resolved Relaxation of the First Excitonic State in CdSe Quantum Dots Probed with near-Infrared Transient Absorption Spectroscopy. *J. Phys. Chem. B* **2010**, *114*, 14514−14520.
(35) Yang, Y.; Rodriguez-Cordoba, W.; Lian, T. Ultrafast Charge Separation and Recombination Dynamics in Lead Sulfide Quantum Dot-Methylene Blue Complexes Probed by Electron and Hole Intraband Transitions. *J. Am. Chem. Soc.* **2011**, *133*, 9246−9249.
(36) Bang, J.; Park, J.; Velu, R.; Yoon, E.; Lee, K.; Cho, S.; Cha, S.; Chae, G.; Joo, T.; Kim, S. Photoswitchable Quantum Dots by Controlling the Photoinduced Electron Transfers. *Chem. Commun.* **2012**, *48*, 9174−9176.
(37) Boulesbaa, A.; Issac, A.; Stockwell, D.; Huang, Z.; Huang, J.; Guo, J.; Lian, T. Ultrafast Charge Separation at CdS Quantum Dot/Rhodamine B Molecule Interface. *J. Am. Chem. Soc.* **2007**, *129*, 15132−15133.
(38) Laviron, E. Electrochemical Reactions with Protonations at Equilibrium 0.10. The Kinetics of the Para-Benzoquinone Hydroquinone Couple on a Platinum-Electrode. *J. Electroanal. Chem.* **1984**, *164*, 213−227.
(39) Giros, B.; Caron, M. G. Molecular Characterization of the Dopamine Transporter. *Trends Pharmacol. Sci.* **1993**, *14*, 43−49.
(40) Usiello, A.; Baik, J. H.; Rouge-Pont, F.; Picetti, R.; Dierich, A.; LeMeur, M.; Piazza, P. V.; Borrelli, E. Distinct Functions of the Two Isoforms of Dopamine D-2 Receptors. *Nature* **2000**, *408*, 199−203.
(41) Darvas, M.; Palmiter, R. D. Restricting Dopaminergic Signaling to Either Dorsolateral or Medial Striatum Facilitates Cognition. *J. Neurosci.* **2010**, *30*, 1158−1165.
(42) Tajima, H.; Li, G. Synthesis of Hydroxyalkyl Isothiocyanates. *Synlett* **1997**, *7*, 773−774.
(43) Clapp, A. R.; Medintz, I. L.; Mauro, J. M.; Fisher, B. R.; Bawendi, M. G.; Mattoussi, H. Fluorescence Resonance Energy Transfer between Quantum Dot Donors and Dye-Labeled Protein Acceptors. *J. Am. Chem. Soc.* **2004**, *126*, 301−310.
(44) Oh, E.; Susumu, K.; Blanco-Canosa, J. B.; Medintz, I. L.; Dawson, P. E.; Mattoussi, H. Preparation of Stable Maleimide-Functionalized Au Nanoparticles and Their Use in Counting Surface Ligands. *Small* **2010**, *6*, 1273−1278.
(45) Vijayendran, R. A.; Ligler, F. S.; Leckband, D. E. A Computational Reaction-Diffusion Model for the Analysis of Transport-Limited Kinetics. *Anal. Chem.* **1999**, *71*, 5405−5412.
(46) Liu, D. S.; Liu, H. J.; Zhou, Y. C.; Yang, Y.; Wang, W. X.; Qu, L.; Chen, C.; Zhang, D. Q.; Zhu, D. B. Photo-pH Dually Modulated Fluorescence Switch Based on DNA Spatial Nanodevice. *J. Phys. Chem. B* **2008**, *112*, 6893−6896.
(47) Kim, B. H.; Shin, K.; Kwon, S. G.; Jang, Y.; Lee, H.-S.; Lee, H.; Jun, S. W.; Lee, J.; Han, S. Y.; Yim, Y.-H.; Kim, D.-H.; Hyeon, T. Sizing by Weighing: Characterizing Sizes of Ultrasmall-Sized Iron Oxide Nanocrystals Using MALDI-TOF Mass Spectrometry. *J. Am. Chem. Soc.* **2013**, *135*, 2407−2410.
(48) Moreels, I.; Fritzinger, B.; Martins, J. C.; Hens, Z. Surface Chemistry of Colloidal PbSe Nanocrystals. *J. Am. Chem. Soc.* **2008**, *130*, 15081−15086.
(49) Salorinne, K.; Lahtinen, T.; Koivisto, J.; Kalenius, E.; Nissinen, M.; Pettersson, M.; Häkkinen, H. Nondestructive Size Determination of Thiol-Stabilized Gold Nanoclusters in Solution by Diffusion Ordered NMR Spectroscopy. *Anal. Chem.* **2013**, *85*, 3489−3492.
(50) Pons, T.; Medintz, I. L.; Wang, X.; English, D. S.; Mattoussi, H. Solution-Phase Single Quantum Dot Fluorescence Resonance Energy Transfer. *J. Am. Chem. Soc.* **2006**, *128*, 15324−15331.
(51) Sapsford, K. E.; Pons, T.; Medintz, I. L.; Higashiya, S.; Brunel, F. M.; Dawson, P. E.; Mattoussi, H. Kinetics of metal-affinity driven self-assembly between proteins or peptides and CdSe-ZnS quantum dots. *J. Phys. Chem. C* **2007**, *111*, 11528−11538.
(52) Zhu, H.; Song, N.; Lian, T. Charging of Quantum Dots by Sulfide Redox Electrolytes Reduces Electron Injection Efficiency in Quantum Dot Sensitized Solar Cells. *J. Am. Chem. Soc.* **2013**, *135*, 11461−4.
(53) Tvrdy, K.; Frantsuzov, P. A.; Kamat, P. V. Photoinduced Electron Transfer from Semiconductor Quantum Dots to Metal Oxide Nanoparticles. *Proc. Natl. Acad. Sci. U.S.A.* **2011**, *108*, 29−34.
(54) Zhang, J. Z. Interfacial Charge Carrier Dynamics of Colloidal Semiconductor Nanoparticles. *J. Phys. Chem. B* **2000**, *104*, 7239−7253.
(55) Klimov, V. I. Optical Nonlinearities and Ultrafast Carrier Dynamics in Semiconductor Nanocrystals. *J. Phys. Chem. B* **2000**, *104*, 6112−6123.
(56) Murray, C. B.; Norris, D. J.; Bawendi, M. G. Synthesis and Characterization of Nearly Monodisperse CdE (E = S, Se, Te) Semiconductor Nanocrystallites. *J. Am. Chem. Soc.* **1993**, *115*, 8706−8715.
(57) Peng, Z. A.; Peng, X. G. Formation of High-Quality CdTe, CdSe and CdS Nanocrystals Using CdO as Precursor. *J. Am. Chem. Soc.* **2001**, *123*, 183−184.
(58) Yu, W. W.; Peng, X. G. Formation of High-Quality CdS and Other II-VI Semiconductor Nanocrystals in Noncoordinating Solvents: Tunable Reactivity of Monomers. *Angew. Chem., Int. Ed.* **2002**, *41*, 2368−2371.
(59) Clapp, A. R.; Goldman, E. R.; Mattoussi, H. Capping of CdSe-ZnS Quantum Dots with DHLA and Subsequent Conjugation with Proteins. *Nat. Protoc.* **2006**, *1*, 1258−1266.
(60) Mattoussi, H.; Cumming, A. W.; Murray, C. B.; Bawendi, M. G.; Ober, R. Properties of CdSe Nanocrystal Dispersions in the Dilute Regime: Structure and Interparticle Interactions. *Phys. Rev. B* **1998**, *58*, 7850−7863.
(61) Susumu, K.; Uyeda, H. T.; Medintz, I. L.; Pons, T.; Delehanty, J. B.; Mattoussi, H. Enhancing the Stability and Biological Functionalities of Quantum Dots Via Compact Multifunctional Ligands. *J. Am. Chem. Soc.* **2007**, *129*, 13987−13996.
(62) Mei, B. C.; Susumu, K.; Medintz, I. L.; Delehanty, J. B.; Mountziaris, T. J.; Mattoussi, H. Modular Poly(Ethylene Glycol) Ligands for Biocompatible Semiconductor and Gold Nanocrystals with Extended pH and Ionic Stability. *J. Mater. Chem.* **2008**, *18*, 4949−4958.
(63) Susumu, K.; Mei, B. C.; Mattoussi, H. Multifunctional Ligands Based on Dihydrolipoic Acid and Polyethylene Glycol to Promote Biocompatibility of Quantum Dots. *Nat. Protoc.* **2009**, *4*, 424−436.
(64) Susumu, K.; Uyeda, H. T.; Medintz, I. L.; Mattoussi, H. Design of Biotin-Functionalized Luminescent Quantum Dots. *J. Biomed. Biotechnol.* **2007**, 90651, DOI: 10.1155/2007/90651.
(65) Leatherdale, C. A.; Woo, W. K.; Mikulec, F. V.; Bawendi, M. G. On the Absorption Cross Section of CdSe Nanocrystal Quantum Dots. *J. Phys. Chem. B* **2002**, *106*, 7619−7622.
(66) Zoski, C. G. *Handbook of Electrochemistry*, 1st ed.; Elsevier: New York, 2007; Chapter 9.

DOI: 10.1021/jp511178u
J. Phys. Chem. C 2015, 119, 3388−3399